Detecting One-Dimensional Dipolar Bosonic Crystal Orders via Full Distribution Functions

Budhaditya Chatterjee,[1,*] Camille Lévêque,[2,3,†] Jörg Schmiedmayer,[2,‡] and Axel U. J. Lode[4,2,3,§]
[1]Department of Physics, Indian Institute of Technology-Kanpur, Kanpur 208016, India
[2]Vienna Center for Quantum Science and Technology, Atominstitut, TU Wien, Stadionallee 2, 1020 Vienna, Austria
[3]Wolfgang Pauli Institute c/o Faculty of Mathematics, University of Vienna, Oskar-Morgenstern Platz 1, 1090 Vienna, Austria
[4]Institute of Physics, Albert-Ludwig University of Freiburg, Hermann-Herder-Strasse 3, 79104 Freiburg, Germany

(Received 8 May 2019; accepted 8 July 2020; published 26 August 2020)

We explore the ground states of a few dipolar bosons in optical lattices with incommensurate filling. The competition of kinetic, potential, and interaction energies leads to the emergence of a variety of crystal state orders with characteristic one- and two-body densities. We probe the transitions between these orders and construct the emergent state diagram as a function of the dipolar interaction strength and the lattice depth. We show that the crystal state orders can be observed using the full distribution functions of the particle number extracted from simulated single-shot images.

DOI: 10.1103/PhysRevLett.125.093602

The realization of Bose-Einstein condensates (BECs) of dipolar atoms [1–6] and molecules [5,6] provides new perspectives to study phase transitions in correlated quantum systems [7,8]. The anisotropic and long-ranged dipole-dipole interactions lead to a plethora of new phenomena absent in conventional BEC, e.g., directional elongation [9–11] and geometric stabilization [9,10,12–14]. A lower dimensionality results in additional physical features: p-wave superfluidity [15,16], Luttinger-liquid-like behavior [17–20], and anisotropy in curved geometries [21–23].

Atoms in optical lattices are experimentally very tunable and serve as quantum simulators for condensed matter systems [24–39]. Few-particle systems especially provide an experimental bottom-up access to many-body physics [40–42]. The interplay between anisotropic long-range and contact interactions result in the emergence of new phases beyond the usual superfluid (SF) and Mott insulator (MI) phases. A density-wave phase (DW) [43–46], characterized by an alternate filling of lattice sites and a supersolid phase [45,47–51], with coexistent DW and superfluidity were observed. Exotic phases such as Haldane insulators [44,52], checkerboards [43,53], and Mott solids [54] were predicted. Remarkably, a crystal state (CS) emerges for dominant dipolar interactions [17,21,22,55–61].

In this Letter, we establish protocols to detect the remarkable plethora of crystal orders emerging in lattices incommensurately filled with dipolar bosons. The physics of the crystal state cannot be addressed using the Hubbard model [62] and requires an *ab initio* many-body description [60,61]. We study ground states of a few dipolar atoms in one-dimensional lattices by numerically solving the full Schrödinger equation with the multiconfigurational time-dependent Hartree method for bosons [63–68].

Like Refs. [69–77], we explore the full range of interaction strengths to observe distinct crystal orders, emergent due to the competition between kinetic, potential, and interaction energies. Our main finding is that all these crystal orderings and, thereby, the phase diagram can be unequivocally characterized using the full distribution functions (FDF) of the position-dependent particle number operator extracted from absorption or single-shot images [60,78–80]. We emphasize that our results are experimentally feasible as single-shot images with single-atom sensitivity for few-atom systems have been observed [81,82]. With our present finite-size considerations, we cannot make claims about the true quantum phases in the thermodynamic limit. However, we demonstrate that the crystal orders are valid for the state diagram, the finite-size analog of the thermodynamic phase diagram for different lattice sizes, particle numbers, and different types of boundary conditions [83].

Consider polarized, dipolar bosons in a quasi-one-dimensional lattice potential having tight transversal confinement of characteristic length $a_\perp$. The N-body Hamiltonian reads

$$H = \sum_{i=1}^{N} [T_i + V_{ol}(x_i)] + \sum_{i<j} V_{\mathrm{int}}(x_i - x_j). \qquad (1)$$

Here, T_i is the kinetic energy of the ith boson, $V_{ol} = V \sin^2(\kappa x)$ is the lattice potential with a depth V and a wave vector κ. Hard-wall boundaries at $x = \pm S\pi/2\kappa$ restrict the lattice to S sites. $V_{\mathrm{int}}(x_i - x_j) = (g_d/|x_i - x_j|^3 + \alpha)$ is the (purely) dipolar interaction of strength g_d [84]. The transversal confinement introduces the short-scale cutoff $\alpha \approx {a_\perp}^3$ [56,85–87]. All quantities are given in terms of

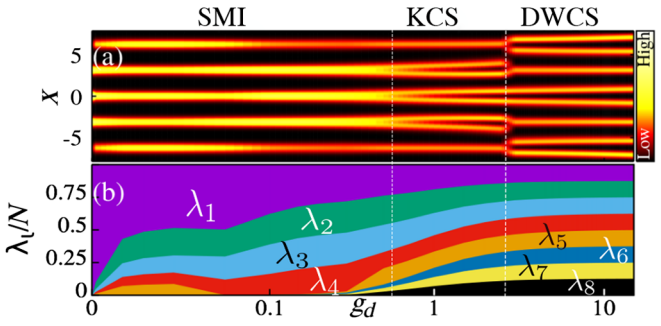

FIG. 1. (a) One-body density $\rho(x)$ as a function of the dipolar interaction strength g_d for a lattice depth $V = 8$. For the SMI, $g_d \lesssim 0.8$, the density exhibits a fivefold structure. As g_d increases, the density develops a twofold splitting in the doubly-occupied central three wells displaying the onset of SMI → KCS transition. For even larger g_d, the density transitions to a pattern with alternating single and double occupations signifying the DWCS transition. See the Supplemental Material [83], Section S2, for $\rho(k)$ in momentum space. (b) Natural occupations (plotted cumulatively) as a function of g_d. For small g_d, the SF fraction results in the dominance of λ_1. With increasing g_d, the fragmentation increases as several $\lambda_{k>1}$ become significant. Beyond the SMI → KCS transition, the system is maximally fragmented with eight almost equally contributing eigenvalues.

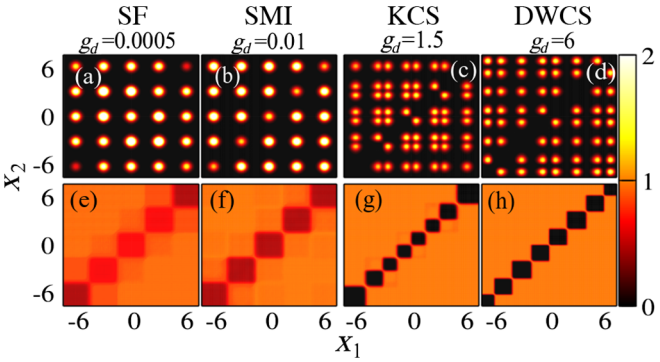

FIG. 2. (a)–(d) Two-body density $\rho^{(2)}(x_1, x_2)$. (a) $g_d = 0.0005$: the pure SF shows a nearly square-lattice-like equispaced distribution. (b) $g_d = 0.01$: the localization of bosons in the SMI results in a diagonal depletion. (c) $g_d = 1.5$: for KCS, a correlation hole develops; the probability to find two bosons at the same position vanishes. (d) $g_d = 6.0$: the DWCS shows a completely split but nonuniform density with density-wave order. (e)–(h): second-order spatial correlation function $[|g^{(2)}(x_1, x_2)|]$. (e) $g_d = 0.0005$: the bosons are significantly coherent for the SF. (f) $g_d = 0.01$: reduction of off-diagonal coherence for the SMI. (g) $g_d = 1.5$: diagonal coherent blocks split as the bosons crystalize at the KCS. (h) $g_d = 6$: completely split coherent blocks centered at each boson position in the DWCS.

recoil energy [88]. We consider a cutoff $\alpha = 0.05$, $N = 8$ bosons, and $S = 5$ lattice sites [89].

We now discuss possible crystal-state orderings using the density $\rho(x) = \langle\Psi|\hat{\Psi}^\dagger(x)\hat{\Psi}(x)|\Psi\rangle$ as a function of the interaction strength g_d [Fig. 1(a)]. For $g_d = 0$, we obtain a pure SF. The incommensurate setup implies the absence of a pure MI; as g_d increases, we find an MI coexisting with an SF (SMI) [90]. Observed from $\rho(x)$: the two outer wells have a smaller population than the central wells; $N = 5$ atoms in the MI coexist with $N = 3$ bosons in the SF fraction. The SF localizes in the central wells to minimize the kinetic energy with hard-wall boundary conditions.

The crystal transition occurs at $g_d \approx 0.8$: due to their repulsive dipolar interactions, the bosons avoid each other and save interaction energy minimizing their overlap. The density [Fig. 1(a)] splits in the doubly occupied central wells - a signature of the crystal transition. The crystal state's site occupations are 1,[11],[11],[11],1, where [11] denotes the two-hump density in doubly-occupied lattice sites. Since the double occupation of the three central wells results from the kinetic energy in the Hamiltonian, we term this state "kinetic crystal state" (KCS).

A further increase in g_d makes the interaction energy overcome the kinetic energy; the double occupation of adjacent sites is energetically unfavorable [Fig. 1(a)]: instead nearest and next-nearest neighbors are now doubly occupied in a density-wave-ordered structure at $g_d \gtrsim 3$. The "standard" density-wave-order for our system would have the occupations 2,1,2,1,2 (Ref. [46]). Due to the strong dipolar interactions, the bosons' density in doubly occupied sites is spatially split and a density-wave crystal state (DWCS) with occupations [11],1,[11],1,[11] results. The DWCS represents a completely new crystal order, featuring the coexistence of DW arrangement and crystallization. The KCS and the DWCS are possible crystal orders and hence a subset of a general CS. Here, and henceforth, we use the label CS for a crystal state in either the KCS or the DWCS arrangement. See Ref. [83], Sections S4, S5, and S9, for finite-size and boundary-condition effects on the crystal orders; importantly, the KCS fades away for a larger system size while the DWCS and CS prevail.

Various crystal arrangements of the atoms with respect to the lattice can be obtained from a purely classical model ([83], Section S4). However, many-body calculations are necessary to capture the quantum properties of the crystal states: many modes contribute to the quantum field of the crystal states [Fig. 1(b)]—their properties are only accessible via a realistic model of the many-body wave function. Moreover, the SF and MI are purely quantum states and the transition from such a noncrystal to a crystal order cannot be obtained from a classical model.

To explain the emergent many-body properties and the localization in the observed states, we discuss the two-body density $\rho^{(2)}(x_1, x_2) = \langle\Psi|\hat{\Psi}^\dagger(x_1)\hat{\Psi}^\dagger(x_2)\hat{\Psi}(x_1)\hat{\Psi}(x_2)|\Psi\rangle$ for characteristic values of g_d [Figs. 2(a)–2(d)]. Unlike the corresponding particle arrangement [one-body density, Fig. 1(a)], the analysis of the two-body density exhibits the many-bodiness of the crystal state: the two-body densities in Figs. 2(b)–2(d) - unlike for classical, semiclassical, and mean-field models - is not a product of one-body densities.

For small interaction strength ($g_d = 0.0005$) in the SF the maxima of $\rho^{(2)}$ are nearly uniformly distributed at positions (x_1, x_2) in the vicinity of the minima of the lattice [Fig. 2(a)]. For larger interaction, $g_d = 0.01$, a partial depletion along the diagonal $(x_1, x_2 \approx x_1)$ of $\rho^{(2)}$ occurs. This depletion results from the formation of an MI that coexists with an SF [Fig. 2(b)]. At stronger interactions, $g_d = 1.5$, the bosons in the doubly occupied central wells crystallize forming the KCS. The diagonal $\rho^{(2)}(x_1, x_1) \approx 0$ is completely depleted: a correlation hole is formed, the probability of detecting two bosons at the same position vanishes. The split maxima in the three central wells result from the on site interaction-driven splitting $2 \to [11]$. For $g_d = 6$, in the DWCS [Fig. 2(d)], a split intersite structure of the two-body density $\rho^{(2)}$ is present for every odd site of the lattice potential. The diagonal depletion is wider compared to the KCS [Figs. 2(c) and 2(d) for $x_1 \approx x_2$]. The nonuniform distribution of the maxima of $\rho^{(2)}$ heralds the DWCS.

For extremely strong interactions $g_d > 50$ (not shown), the DWCS transforms into a pure CS [60,61]. To minimize the interaction that overwhelms the potential, the distribution of the maxima of both $\rho(x)$ and $\rho^{(2)}(x_1, x_2)$ becomes equidistant ([83], Section S3). This pure CS differs from the SMI, KCS, and the DWCS, because the distribution of maxima of the densities is *not* dictated by the minima of the lattice potential (see [83], Sections S4, S5, S9) for other possible crystal orders at different particle numbers, lattice sizes, and boundary conditions.

To explore the coherence properties of the emergent states, we analyze the second-order spatial (Glauber) correlation functions [91,92], defined as $g^{(2)}(x_1,x_2,x_1',x_2')=\rho^{(2)}(x_1,x_2,x_1',x_2')/\sqrt{\rho(x_1)\rho(x_1')\rho(x_2)\rho(x_2')}$ and it quantifies the second-order coherence in the system. Figures 2(e)–2(h) display the diagonal $|g^{(2)}|\equiv|g^{(2)}(x_1,x_2)|=|g^{(2)}(x_1,x_2,x_1'=x_1,x_2'=x_2)|$.

In the SF ($g_d = 0.0005$), the system is delocalized and shows substantial coherence [$|g^{(2)}| \approx 1$ almost throughout Fig. 2(e)]. For the SMI, $g_d = 0.01$, a partial localization in the lattice sites reduces the off-diagonal coherence, reflected in the diagonal anticorrelation blocks $|g^{(2)}| < 1$, Fig. 2(f). For $g_d = 1.5$ (KCS), the diagonal coherent blocks split as the bosons crystallize. The (anti)correlation regions are now centered on each boson [Fig. 2(g)]; this also persists for the DWCS [$g_d = 6$, Fig. 2(h)], showing the complete localization and decoherence of atoms in crystal states. These coherence properties are inherently a quantum many-body effect absent in mean-field approaches ([83], Section S8). The two-body correlation functions and densities in Fig. 2, as expected for multiple significant eigenvalues of the reduced one-body density matrix [Fig. 1(b) and below] demonstrate the appealing many-body structure of crystallized bosons.

The SMI → KCS and KCS → DWCS transitions depend on g_d and V; we construct the state diagram for these parameters. The SMI → CS transition can be determined from a crystal state order parameter Δ [60],

$$\Delta = \sum_k \left(\frac{\lambda_k}{N}\right)^2. \tag{2}$$

Here, the λ_ks are the k eigenvalues (natural occupations) obtained from diagonalizing the one-body reduced density matrix,

$$\rho^{(1)}(x,x') = \langle\Psi|\hat{\Psi}^\dagger(x)\hat{\Psi}(x')|\Psi\rangle = \sum_i \lambda_i \varphi_i^*(x)\varphi_i(x'), \tag{3}$$

together with the eigenfunctions $\varphi_i(x)$ (natural orbitals).

The system is condensed if one natural occupation is macroscopic ($\lambda_1 \approx N$) [93] and fragmented when multiple λ_ks are macroscopic [94,95]. Figure 1(b) shows λ_k as a function of g_d. For $0 < g_d < 0.002$, the system is a condensed SF and $\lambda_1 \approx N$. For $0.002 < g_d < 0.8$, the system fragments and multiple $\lambda_{k>1}$ gradually increase for increasing interactions. At $g_d \gtrsim 0.8$, the CS is reached with N natural orbitals (almost) equally populated [Fig. 1(b)]. It is a hallmark of the many-body properties of the CS: the high-order density matrices [96], $\rho^{(p)}(p > 1)$, are not a product of densities $\rho^{(1)}(x, x')$ [Fig. 2]. Thus, observables such as the correlation functions and the full distribution functions (see below) require a many-body model while classical models fail, see Section S5 [83].

The maximal value of the crystal order parameter, Eq. (2), is obtained for the SF with $\Delta = 1$, while the CS is identified by the minimum value, $\Delta = (1/N) = 0.125$, hence, characterizing the CS transition. Figure 3(a) shows the value of Δ as a function of g_d and V, which clearly displays the transition from the SMI to the CS.

For small g_d and V, the bosons are condensed into a SF and $\Delta \approx 1$. With increasing g_d and/or V, the SMI forms; fragmentation and—consequently—a diminution of Δ is seen. A further increase of g_d (>0.8) decreases Δ gradually towards its minimum value ($\Delta = 0.125$) for all values of V marking the onset of the KCS. When Δ reaches its minimum, the maximally (eightfold) fragmented CS is reached; the orderings of the CS, analyzed in the following, are the KCS or the DWCS. Importantly, by analyzing Δ alone, the KCS → DWCS transition cannot be identified.

To identify the KCS → DWCS, we use the population imbalance of even (e) and odd (o) sites, defined as

$$\Theta = \frac{1}{N}\sum_{e,o}\langle n_o\rangle - \langle n_e\rangle, \tag{4}$$

with $\langle n_e\rangle$ and $\langle n_o\rangle$ as their, respective, populations. Θ is maximal for the density modulation corresponding to the DWCS. Figure 3(b) shows Θ as a function of g_d and V. For small values of g_d, the localization of the atoms in the central wells leads to small values of Θ. For larger g_d, Θ decreases because of the uniform density of the SMI. As g_d

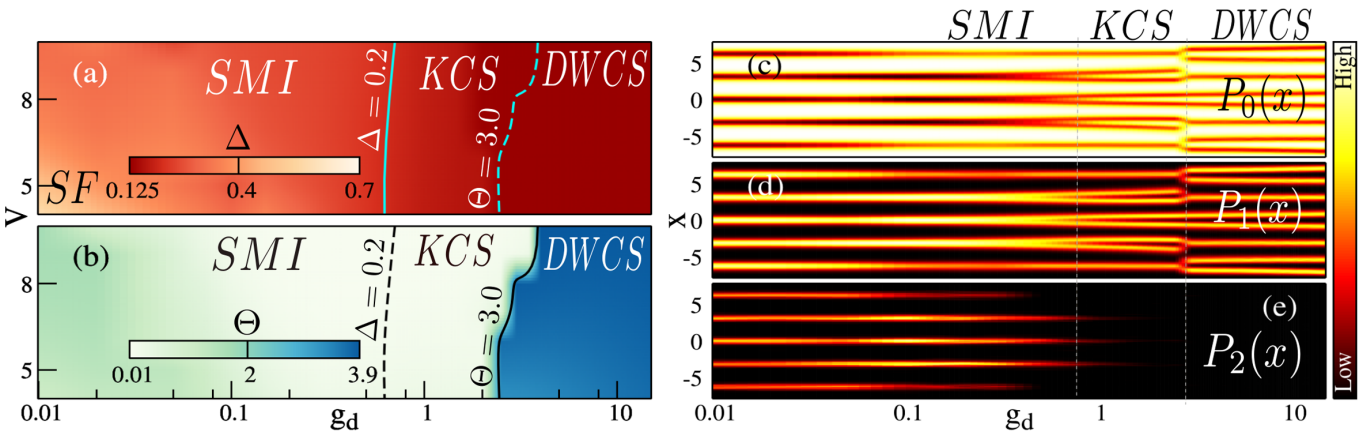

FIG. 3. Characterization and detection of the KCS and DWCS. (a) Crystal order parameter Δ as a function of the interaction strength g_d and lattice depth V. The maximum, $\Delta = 1$, corresponds to the condensed SF. The SMI is revealed by intermediate $\Delta < 1$. The minimum value, $\Delta = 0.125$, corresponds to a CS thereby characterizing its formation. (b) Imbalance parameter Θ as a function of g_d and V. Both SMI and KCS correspond to low values of Θ, while the maximum value indicates the KCS $\rightarrow$ DWCS transition. (c)–(e) Full distribution functions $P_n(x)$ as a function of g_d for $V = 8$ evaluated from 10000 single shots. The plots of the probability to detect zero $[P_0(x)]$ or one $[P_1(x)]$ particle are reminiscent of the one-body density [compare Fig. 1(a)]. The probability of detecting two particles $[P_2(x)]$ vanishes clearly when the CS transition occurs. At large interactions, $g_d \gtrsim 6$, $P_0(x)$ and $P_1(x)$ exhibit a density-wave pattern. This pattern along with vanishing $P_2(x)$ reveals the DWCS. See [83], Section S6, for the FDF in momentum space.

increases further, Θ reaches its maximum value for the KCS $\rightarrow$ DWCS transition, which shows a stronger dependence on V compared to the SMI $\rightarrow$ KCS transition. A shallower lattice potential favors the KCS $\rightarrow$ DWCS transition at lower g_d while deeper lattices require larger g_d, Fig. 3(b). The order parameters Δ and Θ quantify state diagram of any finite-size system as they are applicable for any finite N and S.

We now propose a general experimental protocol to detect all emergent states and thereby the state diagram of crystal orders using standard imaging [81,82]. These single-shot measurements correspond to a projective measurement of the wave function. Ideally, the images contain an instantaneous sample of the position of all N particles distributed according to the N-particle probability distribution $|\Psi|^2$. Here, we compute a set of single-shot measurements from our MCTDH-B ground state wave functions [78–80,97] and evaluate the full distribution functions of the position-dependent particle number operator, i.e., we quantify the probability $P_n(x)$ to detect n particles at positions x [Figs. 3(c)–3(e)].

In the delocalized SMI, several particles can be detected in the same site with a significant probability: $P_n(x)$ are nonzero for $n \leq 2$. When the KCS is reached at $g_d \approx 0.8$, the bosons become completely localized resulting in $P_{n\geq 2}(x) \approx 0$. The transition from the SMI via the KCS to the DWCS with increasing interaction strength g_d is characterized unequivocally through the analysis of the full distribution functions $P_0(x)$, $P_1(x)$ and $P_2(x)$. While P_0 and P_1 exhibit the distribution patterns of the KCS and the DWCS, $P_2 \rightarrow 0$ signals the bosons' complete isolation in crystal states—independent of the crystal ordering. The results of Figs. 3(c)–3(e) show a good agreement with the ones of Figs. 1(a) and 3(a) and 3(b), demonstrating the KCS and DWCS transition for the same values of g_d. The simultaneous presence of density-wave order in $P_{0/1}$ and isolation, $P_{n\geq 2} \rightarrow 0$, can thus experimentally identify the KCS and the DWCS (see [83], Section S5, for $P_{n\geq 3} \approx 0$). The FDF as shown in Figs. 3(c)–3(e) is thus sufficient for detecting all the crystal orders and emergent states and, thereby, the order-parameter and state-diagram. Since the FDF has been experimentally implemented [98], our protocol thus provides a general and experimentally feasible way to explore the plethora of crystal orders of dipolar bosons in a lattice.

We emphasize that our crystal-order detection protocol using FDFs makes no reference to N or S: it thus represents a viable method for *any* finite-size system.

We note that finite-size cold-atom systems necessarily exhibit pinning, thus precluding difficulties arising due to sliding phases that may be seen for periodic boundary conditions ([83], Section 9). Moreover, the required accurate single-shot imaging techniques with high detection efficiency and close-to-single-atom detection are available for ultracold atoms [81].

An alternative experimental protocol using the variance of single-shot measurements to quantify the order parameter Δ [60,79] intertwined with a binning of them to quantify the even-odd imbalance Θ is described in [83], Section S7.

Beyond the static properties, the exploration of collective excitations like roton modes which have been theoretically predicted [46,99–102] and experimentally observed [103–105] would be of further interest.

We expect low lying phononlike excitations in our many-body system, similarly to [99]. In contrast to [99], the dependence of the crystal spacing on the strength of the dipole-dipole interactions alters the dispersion relation and, therewith, the phonon modes in our setup.

B. C. acknowledges the financial support from Department of Science and Technology, Government of India under DST Inspire Faculty fellowship. A. U. J. L. and C. L. acknowledge financial support by the Austrian Science Foundation (FWF) under Grants No. P-32033-N32 and No. M-2653, respectively. J. S. and A. U. J. L. acknowledges funding from the Wiener Wissenschafts-und Technologie Funds (WWTF) Project No. MA16-066. Computation time on the HPC2013 cluster of the IIT Kanpur and the HazelHen and Hawk clusters at the HLRS Stuttgart, as well as support by the state of Baden-Württemberg through bw's high performance computation clusters (bwHPC) and the German Research Foundation (DFG) through Grants No. INST 40/467-1 FUGG (JUSTUS cluster), No. INST 39/963-1 FUGG (bwForCluster NEMO), and No. INST 37/935-1 FUGG (bwForCluster BinAC) is gratefully acknowledged.

*bchat@iitk.ac.in
†camille.leveque@tuwien.ac.at
‡Schmiedmayer@atomchip.org
§auj.lode@gmail.com

[1] A. Griesmaier, J. Werner, S. Hensler, J. Stuhler, and T. Pfau, Phys. Rev. Lett. **94**, 160401 (2005).
[2] Q. Beaufils, R. Chicireanu, T. Zanon, B. Laburthe-Tolra, E. Maréchal, L. Vernac, J.-C. Keller, and O. Gorceix, Phys. Rev. A **77**, 061601(R) (2008).
[3] M. Lu, N. Q. Burdick, S. H. Youn, and B. L. Lev, Phys. Rev. Lett. **107**, 190401 (2011).
[4] K. Aikawa, A. Frisch, M. Mark, S. Baier, A. Rietzler, R. Grimm, and F. Ferlaino, Phys. Rev. Lett. **108**, 210401 (2012).
[5] K. K. Ni, S. Ospelkaus, M. H. G. de Miranda, A. Pe'er, B. Neyenhuis, J. J. Zirbel, S. Kotochigova, P. S. Julienne, D. S. Jin, and J. Ye, Science **322**, 231 (2008).
[6] J. W. Park, S. A. Will, and M. W. Zwierlein, Phys. Rev. Lett. **114**, 205302 (2015).
[7] M. A. Baranov, Phys. Rep. **464**, 71 (2008).
[8] T. Lahaye, C. Menotti, L. Santos, M. Lewenstein, and T. Pfau, Rep. Prog. Phys. **72**, 126401 (2009).
[9] S. Yi and L. You, Phys. Rev. A **63**, 053607 (2001).
[10] L. Santos, G. V. Shlyapnikov, P. Zoller, M. Lewenstein *et al.*, Phys. Rev. Lett. **85**, 1791 (2000).
[11] K. Góral, K. Rzazewski, and T. Pfau, Phys. Rev. A **61**, 051601(R) 2000).
[12] C. Eberlein, S. Giovanazzi, and D. H. J. O'Dell, Phys. Rev. A **71**, 033618 (2005).
[13] K. Góral and L. Santos, Phys. Rev. A **66**, 023613 (2002).
[14] T. Koch, T. Lahaye, J. Metz, B. Fröhlich, A. Griesmaier, and T. Pfau, Nat. Phys. **4**, 218 (2008).
[15] G. M. Bruun and E. Taylor, Phys. Rev. Lett. **101**, 245301 (2008).
[16] N. R. Cooper and G. V. Shlyapnikov, Phys. Rev. Lett. **103**, 155302 (2009).
[17] A. S. Arkhipov, G. E. Astrakharchik, A. V. Belikov, and Y. E. Lozovik, JETP Lett. **82**, 39 (2005).
[18] R. Citro, E. Orignac, S. De Palo, and M. L. Chiofalo, Phys. Rev. A **75**, 051602(R) (2007).
[19] S. De Palo, E. Orignac, R. Citro, and M. L. Chiofalo, Phys. Rev. B **77**, 212101 (2008).
[20] P. Pedri, S. De Palo, E. Orignac, R. Citro, and M. L. Chiofalo, Phys. Rev. A **77**, 015601 (2008).
[21] S. Zöllner, G. M. Bruun, C. J. Pethick, and S. M. Reimann, Phys. Rev. Lett. **107**, 035301 (2011).
[22] S. Zöllner, Phys. Rev. A **84**, 063619 (2011).
[23] M. Maik, P. Buonsante, A. Vezzani, and J. Zakrzewski, Phys. Rev. A **84**, 053615 (2011).
[24] D. Jaksch, C. Bruder, J. I. Cirac, C. W. Gardiner, and P. Zoller, Phys. Rev. Lett. **81**, 3108 (1998).
[25] M. Greiner, O. Mandel, T. Esslinger, T. W. Hänsch, and I. Bloch, Nature (London) **415**, 39 (2002).
[26] M. Di Liberto, A. Hemmerich, and C. Morais Smith, Phys. Rev. Lett. **117**, 163001 (2016).
[27] T. Kock, C. Hippler, A. Ewerbeck, and A. Hemmerich, J. Phys. B **49**, 042001 (2016).
[28] T. Kock, M. Ölschläger, A. Ewerbeck, W. M. Huang, L. Mathey, and A. Hemmerich, Phys. Rev. Lett. **114**, 115301 (2015).
[29] R. Landig, L. Hruby, N. Dogra, M. Landini, R. Mottl, T. Donner, and T. Esslinger, Nature (London) **532**, 476 (2016).
[30] G. Jotzu, M. Messer, R. Desbuquois, M. Lebrat, T. Uehlinger, D. Greif, and T. Esslinger, Nature (London) **515**, 237 (2014).
[31] M. Landini, N. Dogra, K. Kroeger, L. Hruby, T. Donner, and T. Esslinger, Phys. Rev. Lett. **120**, 223602 (2018).
[32] T. Langen, S. Erne, R. Geiger, B. Bauer, T. Schweigler, M. Kuhnert, W. Rohinger, I. E. Mazets, T. Gasenzer, and J. Schmiedmayer, Science **348**, 207 (2015).
[33] T. Schweigler, V. Kasper, S. Erne, B. Rauer, T. Langen, T. Gasenzer, J. Berges, and J. Schmiedmayer, Nature (London) **545**, 323 (2017).
[34] N. J. Engelsen, R. Krishnakumar, O. Hosten, and M. A. Kasevich, Phys. Rev. Lett. **118**, 140401 (2017).
[35] T. Lahaye, T. Pfau, and L. Santos, Phys. Rev. Lett. **104**, 170404 (2010).
[36] L. Dell'Anna, G. Mazzarella, V. Penna, and L. Salasnich, Phys. Rev. A **87**, 053620 (2013).
[37] B. Xiong and U. R. Fischer, Phys. Rev. A **88**, 063608 (2013).
[38] A. Gallemi, M. Guilleumas, R. Mayol, and A. Sanpera, Phys. Rev. A **88**, 063645 (2013).
[39] A. Gallemi, G. Queralto, M. Guilleumas, R. Mayol, and A. Sanpera, Phys. Rev. A **94**, 063626 (2016).
[40] F. Serwane, G. Zürn, T. Lompe, T. B. Ottenstein, A. N. Wenz, and S. Jochim, Science **332**, 336 (2011).
[41] S. Murmann, A. Bergschneider, V. M. Klinkhamer, G. Zürn, T. Lompe, and S. Jochim, Phys. Rev. Lett. **114**, 080402 (2015).

[42] S. Murmann, F. Deuretzbacher, G. Zürn, J. Bjerlin, S. M. Reimann, L. Santos, T. Lompe, and S. Jochim, Phys. Rev. Lett. **115**, 215301 (2015).

[43] K. Góral, L. Santos, and M. Lewenstein, Phys. Rev. Lett. **88**, 170406 (2002).

[44] E. G. Dalla Torre, E. Berg, and E. Altman, Phys. Rev. Lett. **97**, 260401 (2006).

[45] K. Biedroń, M. Łacki, and J. Zakrzewski, Phys. Rev. B **97**, 245102 (2018).

[46] A. Maluckov, G. Gligorić, L. Hadžievski, B. A. Malomed, and T. Pfau, Phys. Rev. Lett. **108**, 140402 (2012).

[47] D. L. Kovrizhin, G. Venketeswara Pai, S. Sinha, G. V. Pai, and S. Sinha, Europhys. Lett. **72**, 162 (2005).

[48] S. Yi, T. Li, and C. P. Sun, Phys. Rev. Lett. **98**, 260405 (2007).

[49] D. Grimmer, A. Safavi-Naini, B. Capogrosso-Sansone, and S. G. Söyler, Phys. Rev. A **90**, 043635 (2014).

[50] F. Cinti, J. Low Temp. Phys. **182**, 153 (2016).

[51] I. Danshita and C. A. R. Sa de Melo, Phys. Rev. Lett. **103**, 225301 (2009).

[52] X. Deng and L. Santos, Phys. Rev. B **84**, 085138 (2011).

[53] C. Menotti, C. Trefzger, and M. Lewenstein, Phys. Rev. Lett. **98**, 235301 (2007).

[54] B. Capogrosso-Sansone, C. Trefzger, M. Lewenstein, P. Zoller, and G. Pupillo, Phys. Rev. Lett. **104**, 125301 (2010).

[55] G. E. Astrakharchik and Yu. E. Lozovik, Phys. Rev. A **77**, 013404 (2008).

[56] F. Deuretzbacher, J. C. Cremon, and S. M. Reimann, Phys. Rev. A **81**, 063616 (2010).

[57] J. Schachenmayer, I. Lesanovsky, A. Micheli, and A. J. Daley, New J. Phys. **13**, 059503 (2010).

[58] S. Bera, B. Chakrabarti, A. Gammal, M. C. Tsatsos, M. L. Lekala, B. Chatterjee, C. Lévêque, and A. U. J. Lode, Sci Rep. **9**, 17873 (2019).

[59] B. Chatterjee, I. Brouzos, L. Cao, and P. Schmelcher, J. Phys. B **46**, 085304 (2013).

[60] B. Chatterjee and A. U. J. Lode, Phys. Rev. A **98**, 053624 (2018).

[61] B. Chatterjee, M. C. Tsatsos, and A. U. J. Lode, New J. Phys. **21**, 033030 (2019).

[62] Hubbard models employ a tight-binding approximation suitable in situations where the energy scales are determined by a lattice potential. For a crystal state, the arrangement of the bosons are determined by dipolar interactions and not by necessarily by the lattice potential. In particular, the wave function forms structures on length scales smaller than the lattice constant.

[63] O. E. Alon, A. I. Streltsov, and L. S. Cederbaum, Phys. Rev. A **77**, 033613 (2008).

[64] A. I. Streltsov, O. E. Alon, and L. S. Cederbaum, Phys. Rev. Lett. **99**, 030402 (2007).

[65] A. U. J. Lode, M. C. Tsatsos, E. Fasshauer, R. Lin, L. Papariello, P. Molignini, C. Lévêque, and S. E. Weiner, MCTDH-X: The time-dependent multiconfigurational Hartree for indistinguishable particles software (2020), http://ultracold.org.

[66] E. Fasshauer and A. U. J. Lode, Phys. Rev. A **93**, 033635 (2016).

[67] A. U. J. Lode, Phys. Rev. A **93**, 063601 (2016).

[68] A. U. J. Lode, C. Lévêque, L. B. Madsen, A. I. Streltsov, and O. E. Alon, Rev. Mod. Phys. **92**, 011001 (2020).

[69] U. R. Fischer, A. U. J. Lode, and B. Chatterjee, Phys. Rev. A **91**, 063621 (2015).

[70] L. Cao, S. I. Mistakidis, X. Deng, and P. Schmelcher, Chem. Phys. **482**, 303 (2017).

[71] S. I. Mistakidis and P. Schmelcher, Phys. Rev. A **95**, 013625 (2017).

[72] G. M. Koutentakis, S. I. Mistakidis, and P. Schmelcher, Phys. Rev. A **95**, 013617 (2017).

[73] S. I. Mistakidis, G. M. Koutentakis, and P. Schmelcher, Chem. Phys. **509**, 106 (2018).

[74] A. I. Streltsov, Phys. Rev. A **88**, 041602(R) (2013).

[75] O. I. Streltsova, O. E. Alon, L. S. Cederbaum, and A. I. Streltsov, Phys. Rev. A **89**, 061602(R) (2014).

[76] S. Klaiman, R. Beinke, L. S. Cederbaum, A. I. Streltsov, and O. E. Alon, Chem. Phys. **509**, 45 (2018).

[77] O. V. Marchukov and U. R. Fischer, Ann. Phys. (Amsterdam) **405**, 274 (2019).

[78] K. Sakmann and M. Kasevich, Nat. Phys. **12**, 451 (2016).

[79] A. U. J. Lode and C. Bruder, Phys. Rev. Lett. **118**, 013603 (2017).

[80] J. H. V. Nguyen, M. C. Tsatsos, D. Luo, A. U. J. Lode, G. D. Telles, V. S. Bagnato, and R. G. Hulet, Phys. Rev. X **9**, 011052 (2019).

[81] W. S. Bakr, J. I. Gillen, A. Peng, S. Fölling, and M. Greiner, Nature (London) **462**, 74 (2009).

[82] J. F. Sherson, C. Weitenberg, M. Endres, M. Cheneau, I. Bloch, and S. Kuhr, Nature (London) **467**, 68 (2010).

[83] See the Supplemental Material at http://link.aps.org/supplemental/10.1103/PhysRevLett.125.093602 about a classical model for dipolar crystal orders and an alternate detection protocol for the phase diagram with the single-shot variance and even-odd-imbalance as well as the full distribution function for $P_{n>2}$ in real and momentum space and a discussion of kinetic, potential, and interaction energy.

[84] The dipolar interaction strength $g_d = d_m^2/4\pi\epsilon_0$ for electric dipoles and $g_d = d_m^2\mu_0/4\pi$ for magnetic dipoles, d_m being the dipole moment, ϵ_0 the vacuum permittivity, and μ_0 the vacuum permeability.

[85] S. Sinha and L. Santos, Phys. Rev. Lett. **99**, 140406 (2007).

[86] Y. Cai, M. Rosenkranz, Z. Lei, and W. Bao, Phys. Rev. A **82**, 043623 (2010).

[87] In general, the dipole-dipole interaction potential in 1D also includes a contact (Dirac delta) term owing to the transverse confinement that can be safely neglected for strong interaction strengths [60].

[88] We make all quantities dimensionless by expressing them in terms of the lattice recoil energy for particles of mass M, $E_R = \hbar^2\kappa^2/2M$. This is equivalent to setting $\hbar = M = \kappa = 1$. All quantities become dimensionless with the length given in units of κ^{-1}.

[89] $\alpha = 0.05$ corresponds to $a_\perp \approx 0.37$ and an aspect ratio $\gamma = (a_\parallel/a_\perp) \approx 42.5$. We impose hard-wall boundary conditions at $x = \pm 5\pi/2$ to restrict our lattice to $S = 5$ sites.

[90] I. Brouzos, S. Zöllner, and P. Schmelcher, Phys. Rev. A **81**, 053613 (2010).

[91] K. Sakmann, A. I. Streltsov, O. E. Alon, and L. S. Cederbaum, Phys. Rev. A **78**, 023615 (2008).
[92] R. J. Glauber, Phys. Rev. **130**, 2529 (1963).
[93] O. Penrose and L. Onsager, Phys. Rev. **104**, 576 (1956).
[94] R. W. Spekkens and J. E. Sipe, Phys. Rev. A **59**, 3868 (1999).
[95] E. J. Mueller, T.-L. Ho, M. Ueda, and G. Baym, Phys. Rev. A **74**, 033612 (2006).
[96] C. Lévêque, F. Diorico, J. Schmiedmayer, A. U. J. Lode, arXiv:2006.10755.
[97] S. I. Mistakidis, G. C. Katsimiga, P. G. Kevrekidis, and P. Schmelcher, New J. Phys. **20**, 043052 (2018).
[98] T. Betz, S. Manz, R. Bücker, T. Berrada, Ch. Koller, G. Kazakov, I. E. Mazets, H.-P. Stimming, A. Perrin, T. Schumm, and J. Schmiedmayer, Phys. Rev. Lett. **106**, 020407 (2011).
[99] A. Maluckov, G. Gligorić, L. Hadžievski, B. A. Malomed, and T. Pfau, Phys. Rev. A **87**, 023623 (2013).
[100] L. Santos, G. V. Shlyapnikov, and M. Lewenstein, Phys. Rev. Lett. **90**, 250403 (2003).
[101] S. Ronen, D. C. E. Bortolotti, and J. L. Bohn, Phys. Rev. Lett. **98**, 030406 (2007).
[102] M. Jona-Lasinio, K. Lakomy, and L. Santos, Phys. Rev. A **88**, 013619 (2013).
[103] R. Mottl, F. Brennecke, K. Baumann, R. Landig, T. Donner, and T. Esslinger, Science **336**, 1570 (2012).
[104] L. Chomaz, R. M. W. van Bijnen, D. Petter, G. Faraoni, S. Baier, J. H. Becher, M. J. Mark, F. Wächtler, L. Santos, and F. Ferlaino, Nat. Phys. **14**, 442 (2018).
[105] D. Petter, G. Natale, R. M. W. van Bijnen, A. Patscheider, M. J. Mark, L. Chomaz, and F. Ferlaino, Phys. Rev. Lett. **122**, 183401 (2019).